

Production of Scalar Higgs Bosons Associated with Z^0 Boson at the CERN LHC in the MSSM

Li Lin Yang,¹ Chong Sheng Li,^{1,*} Jian Jun Liu,¹ and Li Gang Jin²

¹*Department of Physics, Peking University, Beijing 100871, China*

²*Institute of Theoretical Physics, Academia Sinica,*

P. O. Box 2735, Beijing 100080, China

(Dated: May 22, 2019)

Abstract

We study the associated production of a scalar neutral Higgs boson (h^0 or H^0) with Z^0 boson in the minimal supersymmetric extension of the standard model (MSSM) at the CERN Large Hadron Collider (LHC), including the contributions from $b\bar{b}$ annihilation at the tree level and those from gluon fusion via quark and squark loops. We quantitatively analyze the total cross sections in the mSUGRA scenario. We find that in the most of the parameter regions, the total cross sections for associated production of light scalar Higgs boson h^0 and Z^0 boson are increased by several tens of fb compared with previous results for the vector boson bremsstrahlung $q\bar{q} \rightarrow Z^* \rightarrow Zh^0/ZH^0$. And the total cross sections for associated production of heavy scalar Higgs boson H^0 and Z^0 boson, with including the contributions of $b\bar{b}$ channel, can also be increased greatly. Especially for large $\tan\beta$, such increasement can reach about one order of magnitude. Thus, the contributions of $b\bar{b}$ channel and gluon fusion should be taken into account seriously.

PACS numbers: 14.80.Cp, 12.60.Jv, 13.85.Lg

*Electronic address: csli@pku.edu.cn

I. INTRODUCTION

The search for Higgs bosons is one of the main goals of the CERN Large Hadron Collider (LHC), with $\sqrt{s} = 14\text{TeV}$ and a luminosity of 100 fb^{-1} per year [1]. In the standard model (SM), the Higgs boson mass is basically a free parameter with an upper bound of $m_H \leq 600 - 800\text{GeV}$ [2]. However, present data from precision measurements of electroweak quantities indicate the existence of a light Higgs boson ($m_H < 204\text{ GeV}$ at 95% C.L.) and direct searches rule out the case $m_H < 114\text{GeV}$ [3]. In addition, in various extensions of the SM, for example, in the two-Higgs-doublet models (THDM) [4], particularly in the minimal supersymmetric standard model (MSSM) [5], there are five physical Higgs particles: two neutral CP-even h^0 and H^0 bosons, one neutral CP-odd A^0 boson, and two charged H^\pm bosons, the Higgs boson h^0 of which should be lightest, with a mass $m_{h^0} \leq 135\text{GeV}$ when including the radiative corrections [6]. It has been shown [7] that the h^0 boson cannot escape detection at the LHC and that in large areas of the parameter space, more than one Higgs particle can be found.

At the LHC, the neutral Higgs bosons can be produced through following mechanisms: gluon fusion $gg \rightarrow \phi$ [8, 9, 10, 11], weak boson fusion $qq \rightarrow qqV^*V^* \rightarrow qqh^0/qqH^0$ [12], associated production with weak bosons [13], associated production with a heavy quark-antiquark pair $gg, q\bar{q} \rightarrow t\bar{t}\phi/b\bar{b}\phi$ [14] and pairs production [15]. In this paper we focus our attentions on the production associated with Z^0 boson in the MSSM. Apart from the Drell-Yan production process (light $q\bar{q}$ annihilation) which has been studied previously [13], in contrast to the case in the SM, there are potentially important contributions to this process from $b\bar{b}$ annihilation at the tree-level and the gg fusion at one loop in the MSSM, we will investigate these contributions and compare them with ones in the SM.

In the MSSM, the relatively large Yukawa couplings $b-b-\phi$ can enhance Higgs boson production cross section of the process via $b\bar{b}$ annihilation significantly if $\tan\beta$ is large enough. Therefore, besides the production channel via Drell-Yan process, in order to obtain the full tree-level cross sections for the associated production of scalar Higgs bosons with Z^0 boson, the partonic subprocesses $b\bar{b} \rightarrow A^0, G^0 \rightarrow Zh^0/ZH^0$ together with t- and u-channels should also be taken into account. Moreover, due to the large luminosity of gluon at the LHC, the loop induced subprocess $gg \rightarrow Zh^0/ZH^0$ become important, and here should be considered, too. In section II, we list analytical results for the tree level cross sections of

$pp \rightarrow b\bar{b} \rightarrow Zh^0/ZH^0$ and loop induced cross section of $pp \rightarrow gg \rightarrow Zh^0/ZH^0$ in the MSSM. The relevant MSSM couplings and form factors are given in the Appendix. In section III, we present quantitative predictions for the inclusive cross section of $pp \rightarrow Zh^0/ZH^0 + X$ at the LHC adopting the MSSM parameters constrained within the minimal supergravity (mSUGRA) scenario and discuss the implications of our results.

II. CALCULATION

The relevant Feynman diagrams are created by FeynArts [16] version 3.2 automatically and are shown in Fig. 1–3. We carry out the calculation in the 't Hooft–Feynman gauge and use dimensional reduction for regularization of the ultraviolet divergences in the loop diagrams. In the following expressions, $G_{L,R}^{\bar{f}fZ}$ and G^{ijk} are the couplings, which are given explicitly in Appendix A; H stands for the scalar Higgs bosons, h^0 or H^0 ; S and f are propagating scalar and fermion particles, respectively.

For the partonic subprocesses

$$\begin{aligned} b(k_1) + \bar{b}(k_2) &\rightarrow Z(k_3, \varepsilon_3) + H(k_4), \\ g(k_1, \varepsilon_1) + g(k_2, \varepsilon_2) &\rightarrow Z(k_3, \varepsilon_3) + H(k_4), \end{aligned}$$

we define the Mandelstam variables as

$$\hat{s} = (k_1 + k_2)^2, \quad \hat{t} = (k_1 - k_3)^2, \quad \hat{u} = (k_1 - k_4)^2. \quad (1)$$

The tree-level amplitude $\mathcal{M}^{b\bar{b}}$ for the subprocess $b\bar{b} \rightarrow ZH$ consists of the three diagrams (a)–(c) in Fig. 1. The previous results [13] for vector boson bremsstrahlung include only the first diagram, where the $b\bar{b}$ pair replaced by light quark-antiquark pairs. We also recompute the contributions of light quarks to the tree-level cross sections and compare them with ones of $b\bar{b} \rightarrow ZH$.

Using the notations defined above, the amplitude $\mathcal{M}^{b\bar{b}}$ can be expressed as

$$\mathcal{M}^{b\bar{b}} = \mathcal{M}_a^{b\bar{b}} + \mathcal{M}_b^{b\bar{b}} + \mathcal{M}_c^{b\bar{b}} \quad (2)$$

with

$$\mathcal{M}_a^{b\bar{b}} = \bar{v}(k_2) \not{\varepsilon}_3 (G_L^{\bar{b}bZ} P_L + G_R^{\bar{b}bZ} P_R) u(k_1) \frac{-iG^{HZZ}}{\hat{s} - m_Z^2}, \quad (3)$$

$$\mathcal{M}_b^{\bar{b}\bar{b}} = \sum_{S=A^0, G^0} \bar{v}(k_2) G^{\bar{b}\bar{b}S} \gamma^5 u(k_1) \frac{iG^{HSZ}}{\hat{s} - m_S^2 + im_S \Gamma_S} (k_3 + 2k_4) \cdot \varepsilon_3, \quad (4)$$

$$\begin{aligned} \mathcal{M}_c^{\bar{b}\bar{b}} &= \bar{v}(k_2) G^{\bar{b}\bar{b}H} \frac{i(\not{k}_1 - \not{k}_3 + m_b)}{\hat{t} - m_b^2} \not{\varepsilon}_3 (G_L^{\bar{b}\bar{b}Z} P_L + G_R^{\bar{b}\bar{b}Z} P_R) u(k_1) \\ &+ \bar{v}(k_2) \not{\varepsilon}_3 (G_L^{\bar{b}\bar{b}Z} P_L + G_R^{\bar{b}\bar{b}Z} P_R) \frac{i(\not{k}_1 - \not{k}_4 + m_b)}{\hat{u} - m_b^2} G^{\bar{b}\bar{b}H} u(k_1). \end{aligned} \quad (5)$$

Here $P_{L,R} \equiv (1 \mp \gamma^5)/2$, $m_{G^0} = m_Z$, $\Gamma_{G^0} = 0$, and Γ_{A^0} is the decay width of A^0 .

The gluon fusion subprocess is forbidden at tree level. At one-loop level, in general, the cross section will receive contributions from both quark loops and squark loops, as shown in Fig. 2, 3. Note that each diagram actually represents a couple of diagrams with opposite directions of charge flow. However, we find that the contributions from each pair of squark loop diagrams to this process cancel each other due to the opposite signs of momenta. So the gluon fusion cross section arises only from the quark loop diagrams, i.e.,

$$\mathcal{M}^{gg} = \mathcal{M}_a^{gg} + \mathcal{M}_b^{gg} + \dots + \mathcal{M}_h^{gg}, \quad (6)$$

where the subscripts $a - h$ refer to the corresponding diagrams in Fig. 2.

In general, the amplitudes \mathcal{M}^{gg} can be written as a linear combination of the invariants formed by three independent external momenta k_1, k_2, k_3 , polarization vectors of three external gauge bosons $\varepsilon_1, \varepsilon_2, \varepsilon_3$, metric tensor $g^{\mu\nu}$ and Levi-Civita tensor $\epsilon^{\mu\nu\rho\sigma}$, in which the terms without Levi-Civita tensor vanish. Thus, with taking into account the relations $\varepsilon_1 \cdot k_1 = \varepsilon_2 \cdot k_2 = \varepsilon_3 \cdot k_3 = 0$, 24 terms remain in the amplitudes. It is easy to prove the following identity

$$\begin{aligned} g^{\mu\nu} \epsilon^{\rho\sigma\alpha\beta} - g^{\mu\rho} \epsilon^{\nu\sigma\alpha\beta} - g^{\mu\alpha} \epsilon^{\nu\rho\sigma\beta} + g^{\mu\beta} \epsilon^{\nu\rho\sigma\alpha} \\ + g^{\nu\sigma} \epsilon^{\mu\rho\alpha\beta} - g^{\rho\sigma} \epsilon^{\mu\nu\alpha\beta} + g^{\sigma\alpha} \epsilon^{\mu\nu\rho\beta} - g^{\sigma\beta} \epsilon^{\mu\nu\rho\alpha} = 0. \end{aligned} \quad (7)$$

Using it, one can immediately see that not all of the 24 terms are linear independent. Actually, there are only 14 independent ones, and finally the amplitudes can be written as

$$\begin{aligned} \mathcal{M}^{gg} &= A_1 \epsilon^{\varepsilon_1 \varepsilon_2 \varepsilon_3 k_1} + A_2 \epsilon^{\varepsilon_1 \varepsilon_2 \varepsilon_3 k_2} + A_3 \epsilon^{\varepsilon_1 \varepsilon_2 \varepsilon_3 k_3} + A_4 \epsilon^{\varepsilon_1 \varepsilon_2 k_1 k_2} \varepsilon_3 \cdot k_1 + A_5 \epsilon^{\varepsilon_1 \varepsilon_2 k_1 k_2} \varepsilon_3 \cdot k_2 \\ &+ A_6 \epsilon^{\varepsilon_1 \varepsilon_3 k_1 k_3} \varepsilon_2 \cdot k_1 + A_7 \epsilon^{\varepsilon_1 \varepsilon_3 k_1 k_3} \varepsilon_2 \cdot k_3 + A_8 \epsilon^{\varepsilon_2 \varepsilon_3 k_2 k_3} \varepsilon_1 \cdot k_2 + A_9 \epsilon^{\varepsilon_2 \varepsilon_3 k_2 k_3} \varepsilon_1 \cdot k_3 \\ &+ A_{10} \epsilon^{\varepsilon_1 k_1 k_2 k_3} \varepsilon_2 \cdot \varepsilon_3 + A_{11} \epsilon^{\varepsilon_2 k_1 k_2 k_3} \varepsilon_1 \cdot \varepsilon_3 + A_{12} \epsilon^{\varepsilon_3 k_1 k_2 k_3} \varepsilon_1 \cdot \varepsilon_2 \\ &+ A_{13} \epsilon^{\varepsilon_1 \varepsilon_2 k_2 k_3} \varepsilon_3 \cdot k_1 + A_{14} \epsilon^{\varepsilon_1 \varepsilon_2 k_1 k_3} \varepsilon_3 \cdot k_2. \end{aligned} \quad (8)$$

The explicit expressions of the form factors $A_i (i = 1, \dots, 14)$ are shown in Appendix B.

The differential cross sections of the subprocesses are given by

$$\frac{d\hat{\sigma}}{d\hat{t}} = \frac{1}{16\pi\hat{s}(\hat{s} - 4m^2)} \overline{\sum} |\mathcal{M}|^2, \quad (9)$$

where $\mathcal{M} = \mathcal{M}^{b\bar{b}}, m = m_b$ for $b\bar{b}$ channel and $\mathcal{M} = \mathcal{M}^{gg}, m = 0$ for gluon fusion.

Using the standard factorization procedure, the hadronic cross section can be obtained as a convolution of partonic cross sections with corresponding parton distribution functions,

$$\sigma(pp \rightarrow ZH) = \sum_{\alpha,\beta} \frac{1}{1 + \delta_{\alpha\beta}} \int_{\tau_0}^1 dx_1 \int_{\tau_0/x_1}^1 dx_2 \left[f_{\alpha/p}(x_1) f_{\beta/p}(x_2) + (\alpha \leftrightarrow \beta) \right] \hat{\sigma}(\alpha\beta \rightarrow ZH), \quad (10)$$

where $\tau_0 = (m_Z + m_H)^2/s$, \sqrt{s} is the center-of-mass energy of the LHC, α and β denote the initial partons.

Note that it is straightforward to deduce the contribution of gluon fusion process to the production of a standard model Higgs boson associated with Z^0 by replacing the corresponding couplings and propagators, with the loop integrals unchanged.

III. NUMERICAL RESULTS AND CONCLUSIONS

In this section we present some numerical results. The SM input parameters were taken to be [3]: the fine structure constant $\alpha(m_Z) = 1/128.8$, the gauge boson masses $m_W = 80.423\text{GeV}$, $m_Z = 91.188\text{GeV}$, and the top quark mass $m_t = 174.3\text{GeV}$. We use the two-loop evolution of the strong coupling constant $\alpha_s(Q)$ [17, 18] with $\alpha_s(m_Z) = 0.1172$. The leading order CTEQ6 parton distribution functions [19] are used here and the factorization scale is taken to be $\mu = (m_Z + m_H)/2$ for light $q\bar{q}$ and gg initial states, and $\mu = (m_Z + m_H)/4$ for $b\bar{b}$ initial state, as suggested in Ref. [20]. Moreover, in order to improve the perturbative calculations, we take the running mass of bottom quark $m_b(Q)$ evaluated by the NLO formula [21]

$$m_b(Q) = U_6(Q, m_t) U_5(m_t, m_b) m_b(m_b), \quad (11)$$

with $m_b(m_b) = 4.25\text{GeV}$. The evolution factor U_f is

$$\begin{aligned} U_f(Q_2, Q_1) &= \left(\frac{\alpha_s(Q_2)}{\alpha_s(Q_1)} \right)^{d_f} \times \left[1 + \frac{\alpha_s(Q_1) - \alpha_s(Q_2)}{4\pi} J_f \right], \\ d_f &= \frac{12}{33 - 2f}, \\ J_f &= -\frac{8092 - 504f + 40f^2}{3(33 - 2f)^2}. \end{aligned} \quad (12)$$

In addition, in order to improve the perturbation calculations, especially for large $\tan\beta$, we make the following replacement in the tree-level couplings :

$$m_b(Q) \rightarrow \frac{m_b(Q)}{1 + \Delta m_b}, \quad (13)$$

$$\begin{aligned} \Delta m_b = & \frac{2\alpha_s}{3\pi} m_{\tilde{g}} \mu \tan\beta I(m_{\tilde{b}_1}, m_{\tilde{b}_2}, m_{\tilde{g}}) + \frac{h_t^2}{16\pi^2} \mu A_t \tan\beta I(m_{\tilde{t}_1}, m_{\tilde{t}_2}, \mu) \\ & - \frac{g^2}{16\pi^2} \mu M_2 \tan\beta \sum_{i=1}^2 \left[(R_{i1}^{\tilde{t}})^2 I(m_{\tilde{t}_i}, M_2, \mu) + \frac{1}{2} (R_{i1}^{\tilde{b}})^2 I(m_{\tilde{b}_i}, M_2, \mu) \right], \end{aligned} \quad (14)$$

where $h_t = \frac{gm_t}{\sqrt{2}m_W \sin\beta}$, $R^{\tilde{q}}(q = t, b)$ is defined to transform the squark current eigenstates to the mass eigenstates, and

$$I(a, b, c) = \frac{1}{(a^2 - b^2)(b^2 - c^2)(a^2 - c^2)} (a^2 b^2 \log \frac{a^2}{b^2} + b^2 c^2 \log \frac{b^2}{c^2} + c^2 a^2 \log \frac{c^2}{a^2}). \quad (15)$$

And the MSSM parameters involved above, as well as the Higgs masses and mixing angles α , are determined in the mSUGRA scenario as implemented in program package ISAJET 7.69 [22]. The GUT parameters were taken to be $m_0 = 200$ GeV, $A_0 = -100$ GeV, $\mu > 0$ and $m_{1/2}$, $\tan\beta$ were varied to obtain various Higgs masses. It should be noted that in some parameter region, $m_{A^0} > m_Z + m_H$, the momentum of A^0 can approach its mass shell, which will lead to a singularity arising from the A^0 propagator. This can be avoided by introducing the non-zero decay width Γ_{A^0} , which was also calculated by ISAJET.

Fig. 4(a) and 5(a) show the total cross sections of the process $pp \rightarrow Zh^0 + X$ versus the light scalar Higgs boson mass m_{h^0} for $\tan\beta = 4, 15$ and 40. Fig. 4(b) and 5(b) show the dependence of the cross sections on $\tan\beta$ for $m_{h^0} = 105$ and 115 GeV. From Fig. 4 we can see that the $b\bar{b}$ contributions are approximately one order of magnitude smaller than the ones of Drell-Yan process [13], and only increase the total cross sections by about several percents, which are smaller than the QCD corrections to the Drell-Yan process. Fig. 5 shows the contributions of gluon fusion to the cross sections. Comparing with the complete $q\bar{q}$ annihilation ones (i.e. Drell-Yan + $b\bar{b}$), one can see that for a light h^0 (for example, $m_{h^0} = 105$ GeV), the contributions of gluon fusion are about the same as the ones of the $q\bar{q}$ annihilation for low $\tan\beta (\leq 4)$, but with the increasing of $\tan\beta$ from 4 to 10, the former decrease significantly, and become one order of magnitude smaller than the latter in general. Nevertheless, Fig. 4 and Fig. 5 indicate that the contributions of $b\bar{b}$ annihilation and gluon fusion to the total cross sections can reach at least several tens of fb, and these results are still important for future experimental measurement at the LHC.

Fig. 6(a) and 7(a) show the total cross sections of the process $pp \rightarrow ZH^0 + X$ as a function of the heavy scalar Higgs boson mass m_{H^0} for the three representative values of $\tan\beta$. Fig. 6(b) and 7(b) show the dependence of the cross sections on $\tan\beta$ for $m_{H^0} = 200$ and 400 GeV. We find that the $b\bar{b}$ contributions to the total cross sections for the production of heavier neutral Higgs boson can be much larger than the ones of Drell-Yan process for large $\tan\beta$, as shown in Fig. 6. For example, when $\tan\beta = 40$ and $m_{H^0} = 200$ GeV, the $b\bar{b}$ cross section is about 28 fb, while $q\bar{q}$ one is less than 1 fb. Therefore, the $b\bar{b}$ channel provides a dramatic enhancement to the total cross sections, and should definitely be considered. On the other hand, the contributions of gluon fusion are very small (< 1 fb) and can be neglected in the most of cases, as shown in Fig. 7.

In Fig. 8 we present the cross sections of the associated production of the SM Higgs boson H_{SM} and Z^0 boson as a function of $m_{H_{SM}}$. We can see that the contributions of gluon fusion are generally one order of magnitude smaller than the ones of the Drell-Yan process. Moreover, for the comparison of the production rates of H_{SM} , h^0 and H^0 , they are displayed as functions of their masses in Fig. 9, where all the contributions (i.e. Drell-Yan + $b\bar{b}$ + gluon fusion) have been included for $\tan\beta = 4$ and 40, respectively. One can find that no matter what the value of $\tan\beta$ is, the production rate of H^0 is the smallest, the one of h^0 is the largest, and the one of H_{SM} is medium. This feature indicates that the predictions of the associated production of the Higgs bosons and Z^0 boson in the SM and the MSSM are different quantitatively and distinguishable, which is in agreement with the results shown in Ref. [18], where only Drell-Yan contributions are included.

In conclusion, we have calculated the scalar Higgs bosons (h^0, H^0) production in association with Z^0 boson via both $b\bar{b}$ channel and gluon fusion subprocess in the mSUGRA model at the LHC. Our results show that in the most of the parameter regions, the total cross sections for associated production of light scalar Higgs boson h^0 and Z^0 boson are increased by several tens of fb compared with previous results for the vector boson bremsstrahlung $q\bar{q} \rightarrow Z^* \rightarrow Zh^0/ZH^0$ [18]. And the total cross sections for associated production of heavy scalar Higgs boson H^0 and Z^0 boson, with including the contributions of $b\bar{b}$ channel, can also be increased greatly. Especially for large $\tan\beta$, such increasement can reach about one order of magnitude. Thus, the contributions of $b\bar{b}$ channel and gluon fusion should be taken into account seriously.

Acknowledgments

This work was supported in part by the National Natural Science Foundation of China.

APPENDIX A: COUPLINGS

Here we list the relevant couplings appeared in the amplitudes. i, j stand for generation indices and r, s stand for color indices. $s_W, c_W, s_\alpha, c_\alpha, s_\beta, c_\beta, t_\beta, s_{\beta-\alpha}, c_{\beta-\alpha}$ denote sine, cosine and tangent of $\theta_W, \alpha, \beta, \beta - \alpha$, respectively.

$$\begin{aligned}
G_L^{\bar{u}^i u^j Z} &= (-3 + 4s_W^2) \frac{ie\delta^{ij}}{6c_W s_W}, & G_R^{\bar{u}^i u^j Z} &= \frac{2ies_W\delta^{ij}}{3c_W}, \\
G_L^{\bar{d}^i d^j Z} &= -(-3 + 2s_W^2) \frac{ie\delta^{ij}}{6c_W s_W}, & G_R^{\bar{d}^i d^j Z} &= -\frac{ies_W\delta^{ij}}{3c_W}, \\
G^{h^0 ZZ} &= \frac{ieM_W s_{\beta-\alpha}}{c_W^2 s_W}, & G^{H^0 ZZ} &= \frac{ieM_W c_{\beta-\alpha}}{c_W^2 s_W}, \\
G^{u^i \bar{u}^j h^0} &= -\frac{ic_\alpha e\delta^{ij} m_{u^i}}{2M_W s_\beta s_W}, & G^{d^i \bar{d}^j h^0} &= \frac{ies_\alpha \delta^{ij} m_{d^i}}{2c_\beta M_W s_W}, \\
G^{u^i \bar{u}^j H^0} &= -\frac{ies_\alpha \delta^{ij} m_{u^i}}{2M_W s_\beta s_W}, & G^{d^i \bar{d}^j H^0} &= -\frac{ic_\alpha e\delta^{ij} m_{d^i}}{2c_\beta M_W s_W}, \\
G^{u^i \bar{u}^j A^0} &= -\frac{e\delta^{ij} m_{u^i}}{2M_W s_W t_\beta}, & G^{d^i \bar{d}^j A^0} &= -\frac{et_\beta \delta^{ij} m_{d^i}}{2M_W s_W}, \\
G^{u^i \bar{u}^j G^0} &= -\frac{e\delta^{ij} m_{u^i}}{2M_W s_W}, & G^{d^i \bar{d}^j G^0} &= \frac{e\delta^{ij} m_{d^i}}{2M_W s_W}, \\
G^{h^0 A^0 Z} &= \frac{c_{\beta-\alpha} e}{2c_W s_W}, & G^{h^0 G^0 Z} &= \frac{es_{\beta-\alpha}}{2c_W s_W}, \\
G^{H^0 A^0 Z} &= -\frac{es_{\beta-\alpha}}{2c_W s_W}, & G^{H^0 G^0 Z} &= \frac{c_{\beta-\alpha} e}{2c_W s_W}, \\
G^{r\bar{u}^i u_s^j g^a} &= -ig_s \delta^{ij} T_{rs}^a, & G^{\bar{d}^i d^j g^a} &= -ig_s \delta^{ij} T_{rs}^a.
\end{aligned}$$

APPENDIX B: FORM FACTORS

This appendix lists all the coefficient A s appeared in the amplitude of subprocess $gg \rightarrow ZH$, in terms of 3- and 4-points one-loop integrals[23]. The diagrams (a) – (e) refer to those in Fig. 2. For convenience, we define abbreviations of one-loop integrals for each diagram as following,

$$\begin{aligned}
C^{(a)} &= C^{(b)} = C(0, \hat{s}, 0, m_f^2, m_f^2, m_f^2) \\
C^{(c)} &= C(m_H^2, m_Z^2, \hat{s}, m_f^2, m_f^2, m_f^2) \\
D^{(c)} &= D(0, m_H^2, m_Z^2, 0, \hat{t}, \hat{s}, m_f^2, m_f^2, m_f^2)
\end{aligned}$$

$$\begin{aligned}
C^{(d)} &= C(m_Z^2, m_H^2, \hat{s}, m_f^2, m_f^2, m_f^2) \\
D^{(d)} &= D(0, m_Z^2, m_H^2, 0, \hat{u}, \hat{s}, m_f^2, m_f^2, m_f^2) \\
C^{(e)} &= C(0, m_H^2, \hat{t}, m_f^2, m_f^2, m_f^2) \\
D^{(e)} &= D(m_Z^2, 0, m_H^2, 0, \hat{u}, \hat{t}, m_f^2, m_f^2, m_f^2)
\end{aligned}$$

Note that in the following expressions there is an implicit sum over f for $f = t, b$.

For diagram (a) and (b), there are only two coefficients which are not zero, respectively.

$$\begin{aligned}
A_4^{(a)} &= A_5^{(a)} = -\frac{1}{2\pi^2} G^{HZZ} (G_L^{\bar{f}fZ} - G_R^{\bar{f}fZ}) G^{\bar{f}fg_1} G^{\bar{f}fg_2} \frac{1}{\hat{s} - m_Z^2} C_{12}^{(a)} \\
A_4^{(b)} &= A_5^{(b)} = \frac{1}{2\pi^2} G^{HSZ} (G_L^{f\bar{f}S} - G_R^{f\bar{f}S}) G^{\bar{f}fg_1} G^{\bar{f}fg_2} \frac{m_f}{\hat{s} - m_S^2 + im_S \Gamma_S} C_0^{(b)}
\end{aligned}$$

For diagram (c), the coefficients are the following expressions time an overall factor $\frac{1}{8\pi^2} G^{f\bar{f}H} (G_L^{\bar{f}fZ} - G_R^{\bar{f}fZ}) G^{\bar{f}fg_1} G^{\bar{f}fg_2} m_f$

$$\begin{aligned}
A_1 &= 4 [C_0^{(c)} + C_1^{(c)} + C_2^{(c)} - 2D_{00}^{(c)} + \hat{s}(D_{12}^{(c)} + D_{13}^{(c)})] \\
&\quad + (\hat{u} - m_Z^2) [D_0^{(c)} - 2D_2^{(c)} + 4(D_{22}^{(c)} + D_{23}^{(c)})] \\
A_2 &= 2C_0^{(c)} + 4(C_1^{(c)} + C_2^{(c)}) + (\hat{t} - m_Z^2) D_0^{(c)} - 2\hat{s} D_1^{(c)} \\
&\quad + 8D_{00}^{(c)} + 4(m_Z^2 + \hat{s} - \hat{t}) D_{12}^{(c)} + 4\hat{s} D_{13}^{(c)} \\
A_3 &= -2C_0^{(c)} - 4C_1^{(c)} + \hat{s} [D_0^{(c)} - 2D_2^{(c)} - 4(D_{12}^{(c)} + D_{22}^{(c)} + D_{23}^{(c)})] \\
A_4 &= -4 [D_0^{(c)} + D_2^{(c)} + D_3^{(c)} - 2(D_{12}^{(c)} + D_{13}^{(c)})] \\
A_5 &= 4 [D_1^{(c)} + 2(D_{12}^{(c)} + D_{13}^{(c)})] \\
A_6 &= 4 [D_2^{(c)} + D_3^{(c)} + 2(D_{22}^{(c)} + D_{23}^{(c)})] \\
A_7 &= A_9 = -4(D_2^{(c)} + 2D_{22}^{(c)}) \\
A_8 &= -4(D_1^{(c)} + 2D_{12}^{(c)}) \\
A_{10} &= 2(D_0^{(c)} - 2D_3^{(c)} - 4D_{12}^{(c)}) \\
A_{11} &= -2 [D_0^{(c)} + 4D_2^{(c)} - 2D_3^{(c)} + 4(D_{22}^{(c)} + D_{23}^{(c)})] \\
A_{12} &= -2 [D_0^{(c)} - 2D_2^{(c)} - 4(D_{12}^{(c)} + D_{22}^{(c)} + D_{23}^{(c)})] \\
A_{13} &= -4(D_0^{(c)} + D_2^{(c)} - D_3^{(c)} - 2D_{12}^{(c)}) \\
A_{14} &= 4 [D_2^{(c)} - D_3^{(c)} + 2(D_{22}^{(c)} + D_{23}^{(c)})]
\end{aligned}$$

The overall factor for diagram (d) is $\frac{1}{8\pi^2}G^{f\bar{f}H}(G_L^{\bar{f}fZ} - G_R^{\bar{f}fZ})G^{\bar{f}fg_1}G^{\bar{f}fg_2}m_f$, and the coefficients are

$$\begin{aligned}
A_1 &= -2C_0^{(d)} + 4C_2^{(d)} + (m_Z^2 - \hat{u} - 4)D_0^{(d)} + 2\hat{s}D_3^{(d)} \\
&\quad + 8D_{00}^{(d)} + 4(\hat{u} - m_Z^2)D_{12}^{(d)} + 4\hat{u}D_{22}^{(d)} + 4(\hat{u} - \hat{t})D_{23}^{(d)} \\
A_2 &= 4C_2^{(d)} + (m_Z^2 - \hat{t}) \left[D_0^{(d)} - 2D_2^{(d)} - 4(D_{12}^{(d)} + D_{22}^{(d)}) \right] + 8D_{00}^{(d)} - 4\hat{s}(D_{13}^{(d)} + D_{23}^{(d)}) \\
A_3 &= 2C_0^{(d)} + 4C_1^{(d)} - \hat{s} \left[D_0^{(d)} - 2D_2^{(d)} - 4(D_{12}^{(d)} + D_{22}^{(d)} + D_{23}^{(d)}) \right] \\
A_4 &= 4 \left[D_3^{(d)} + 2(D_{13}^{(d)} + D_{23}^{(d)}) \right] \\
A_5 &= -4 \left[D_0^{(d)} + D_1^{(d)} + D_2^{(d)} - 2(D_{13}^{(d)} + D_{23}^{(d)}) \right] \\
A_6 &= -4(D_3^{(d)} + 2D_{23}^{(d)}) \\
A_7 &= A_9 = -4(D_2^{(d)} + 2D_{22}^{(d)}) \\
A_8 &= 4 \left[D_1^{(d)} + D_2^{(d)} + 2(D_{12}^{(d)} + D_{22}^{(d)}) \right] \\
A_{10} &= -2 \left[D_0^{(d)} - 4(D_2^{(d)} + D_{12}^{(d)} + D_{22}^{(d)}) \right] \\
A_{11} &= 2(D_0^{(d)} + 4D_{23}^{(d)}) \\
A_{12} &= 2 \left[D_0^{(d)} - 2D_2^{(d)} - 4(D_{12}^{(d)} + D_{22}^{(d)} + D_{23}^{(d)}) \right] \\
A_{13} &= 2 \left[D_0^{(d)} - D_1^{(d)} - 2D_2^{(d)} - 4(D_{12}^{(d)} + D_{22}^{(d)}) \right] \\
A_{14} &= 4(D_2^{(d)} - 2D_{23}^{(d)})
\end{aligned}$$

For diagram (e), the overall factor is $\frac{1}{8\pi^2}G^{f\bar{f}H}(G_L^{\bar{f}fZ} - G_R^{\bar{f}fZ})G^{\bar{f}fg_1}G^{\bar{f}fg_2}m_f$, and coefficients are

$$\begin{aligned}
A_1 &= -2C_0^{(e)} + (\hat{u} - m_Z^2)D_0^{(e)} + 2(m_Z^2 + \hat{u})D_1^{(e)} + 4\hat{u}D_2^{(e)} + (m_Z^2 + \hat{s} - \hat{u})D_3^{(e)} + 8D_{00}^{(e)} \\
&\quad + 4m_Z^2D_{11}^{(e)} + 4(m_Z^2 + \hat{u})(D_{12}^{(e)} + D_{22}^{(e)}) + 4(\hat{u} - m_Z^2)D_{13}^{(e)} + [4(\hat{u} - m_Z^2) - \hat{s}]D_{23}^{(e)} \\
A_2 &= -2C_0^{(e)} + 8D_{00}^{(e)} + 2(\hat{t} - m_Z^2) \left[D_1^{(e)} + D_2^{(e)} + 2(D_{12}^{(e)} + D_{22}^{(e)}) \right] - 4\hat{s}D_{23}^{(e)} \\
A_3 &= 2\hat{s} \left[D_1^{(e)} + 3D_2^{(e)} + 2(D_{13}^{(e)} + D_{23}^{(e)}) \right] + 2(2\hat{s} - m_Z^2)D_{12}^{(e)} + (\hat{t} - m_Z^2 + 5\hat{s})D_{22}^{(e)} \\
A_4 &= 4(D_3^{(e)} + 2D_{23}^{(e)}) \\
A_5 &= 4(D_2^{(e)} + 2D_{23}^{(e)}) \\
A_6 &= -4 \left[D_3^{(e)} + 2(D_{13}^{(e)} + D_{23}^{(e)}) \right] \\
A_7 &= -4 \left[D_0^{(e)} + 3(D_1^{(e)} + D_2^{(e)}) + 2(D_{11}^{(e)} + 2D_{12}^{(e)} + D_{22}^{(e)}) \right]
\end{aligned}$$

$$\begin{aligned}
A_8 &= 4 \left[D_2^{(e)} + 2(D_{12}^{(e)} + D_{22}^{(e)}) \right] \\
A_9 &= -4 \left[D_1^{(e)} + D_2^{(e)} + 2(D_{11}^{(e)} + 2D_{12}^{(e)} + D_{22}^{(e)}) \right] \\
A_{10} &= 8(D_2^{(e)} + D_{12}^{(e)} + D_{22}^{(e)}) \\
A_{11} &= 8(D_{13}^{(e)} + D_{23}^{(e)}) \\
A_{12} &= -2 \left[D_0^{(e)} + 2D_1^{(e)} + 6D_2^{(e)} + 4(D_{12}^{(e)} + D_{22}^{(e)} + D_{13}^{(e)} + D_{23}^{(e)}) \right] \\
A_{13} &= -4 \left[D_1^{(e)} + 3D_2^{(e)} + 2(D_{12}^{(e)} + D_{22}^{(e)}) \right] \\
A_{14} &= -2 \left[D_0^{(e)} + 2(D_1^{(e)} + D_2^{(e)}) + 4(D_{13}^{(e)} + D_{23}^{(e)}) \right]
\end{aligned}$$

Diagrams (f) – (h) all contribute zero.

-
- [1] F. Gianotti, M. L. Mangano and T. Virdee, CERN-TH/2002-078, hep-ph/0204087.
 - [2] T. Hambye and K. Riesselmann, Phys. Rev. **D55**, 7255 (1997).
 - [3] Particle Data Group (K. Hagiwara *et al.*), Phys. Rev. **D66**, 010001 (2002).
 - [4] N. G. Deshpande and E. Ma, Phys. Rev. **D18**, 2574 (1978); H. Geogi, Hadronic Journal **1**, 155 (1978); H. E. Haber, G. L. Kane and T. Sterling, Nucl. Phys. **B161**, 493 (1979); J. F. Donoghue and L. F. Li, Phys. Rev. **D19**, 945 (1979); L. F. Abbott, P. Sikivie and M. B. Wise, Phys. Rev. **D21**, 1393 (1980); B. McWilliams and L. F. Li, Nucl. Phys. **B179**, 62 (1981).
 - [5] H. E. Haber and G. L. Kane, Phys. Rep. **117**, 75 (1985).
 - [6] H. E. Haber and R. Hempfling, Phys. Rev. Lett. **66**, 1815 (1991); Y. Okada, M. Yamaguchi and T. Yanagida, Prog. Theor. Phys. **85**, 1 (1991); J. Ellis, G. Ridolfi and F. Zwirner, Phys. Lett. **B257**, 83 (1991).
 - [7] A. Djouadi, CERN TH/2003-043, hep-ph/0303097; M. Dittmar, talk given at WHEPP 1999, Pramana 55, 151 (2000); F. Gianotti, talk given at the LHC Committee Meeting, CERN, 5/7/2000.
 - [8] H. Georgi *et al.*, Phys. Rev. Lett. **40**, 692 (1978).
 - [9] M. Spira, A. Djouadi, D. Graudenz and P. Zerwas, Phys. Lett. **B318**, 347 (1993); Nucl. Phys. **B453**, 17 (1995); S. Dawson, A. Djouadi and M. Spira, Phys. Rev. Lett. **77**, 16 (1996); A. Djouadi and M. Spira, Phys. Rev. **D62**, 014004 (2000).
 - [10] R. V. Harlander and W. Kilgore, Phys. Rev. Lett. **88**, 201801 (2002); J. High Energy Phys. **0210**, 017 (2002); C. Anastasiou and K. Melnikov, Nucl. Phys. **B646**, 220 (2002); Phys. Rev.

- D67, 037501 (2003); V. Ravindran, J. Smith and W. L. van Neerven, Nucl. Phys. **B665**, 325 (2003).
- [11] S. Catani, D. de Florian, M. Grazzini and P. Nason, J. High Energy Phys. **0307**, 028 (2003); A. Kulesza, G. Sterman and W. Vogelsang, hep-ph/0309264.
- [12] R. N. Cahn and S. Dawson, Phys. Lett. **B136**, 196 (1984); G. Altarelli, B. Mele and F. Pitolli, Nucl. Phys. **B287**, 205 (1987); T. Han, G. Valencia and S. Willenbrock, Phys. Rev. Lett. **69**, 3274 (1992).
- [13] S. L. Glashow, D. V. Nanopoulos and A. Yildiz, Phys. Rev. **D18**, 1724 (1978); R. Kleiss, Z. Kunszt and W. J. Stirling, Phys. Lett. **B253**, 269 (1991); T. Han and S. Willenbrock, Phys. Lett. **B273**, 167 (1991).
- [14] Z. Kunszt, Nucl. Phys. **B247**, 339 (1984); W. Beenakker *et al.*, Phys. Rev. Lett. **87**, 201805 (2001); Nucl. Phys. **B653**, 151 (2003); S. Dawson *et al.*, Phys. Rev. Lett. **87**, 201804 (2001); Phys. Rev. **D67**, 071503 (2003).
- [15] A. A. Barrientos Bendezú and B. A. Kniehl, Phys. Rev. **D64**, 035006 (2001).
- [16] T. Hahn, Comp. Phys. Comm. **140** 418 (2001);
- [17] S. G. Gorishny *et al.*, Mod. Phys. Lett. **A5**, 2703 (1990); Phys. Rev. **D43**, 1633 (1991); A. Djouadi, M. Spira and P. M. Zerwas, Z. Phys. **C70**, 427 (1996); A. Djouadi, J. Kalinowski and M. Spira, Comput. Phys. Commun. **108**, 56 (1998).
- [18] M. Spira, Fortschr. Phys. **46**, 203 (1998).
- [19] J. Pumplin, D. R. Stump, J. Huston, H. L. Lai, P. Nadolsky and W. K. Tung, J. High Energy Phys. **0207**, 012 (2002).
- [20] F. Maltoni, Z. Sullivan and S. Willenbrock, Phys. Rev. **D67**, 093005 (2003).
- [21] M. Carena, D. Garcia, U. Nierste and C. E. M. Wagner, Nucl. Phys. **B577**, 88 (2000).
- [22] H. Baer *et al.*, Manual of ISAJET version 7.69 at <http://www.phy.bnl.gov/~isajet>; hep-ph/0001086 (1999).
- [23] G. Passarino and M. Veltman, Nucl. Phys. **B160**, 151 (1979); A. Denner, Fortschr. Phys. **41**, 4 (1993).

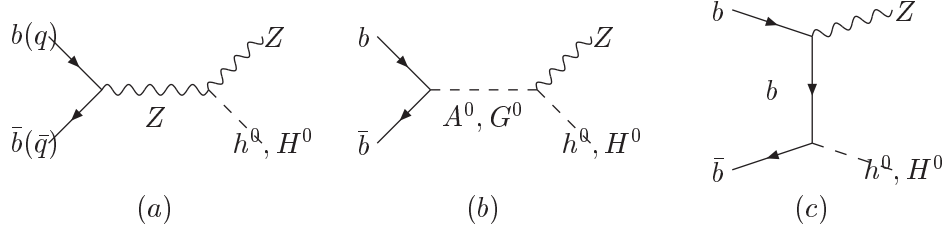


FIG. 1: Feynman diagrams for the subprocess $b\bar{b} \rightarrow ZH$

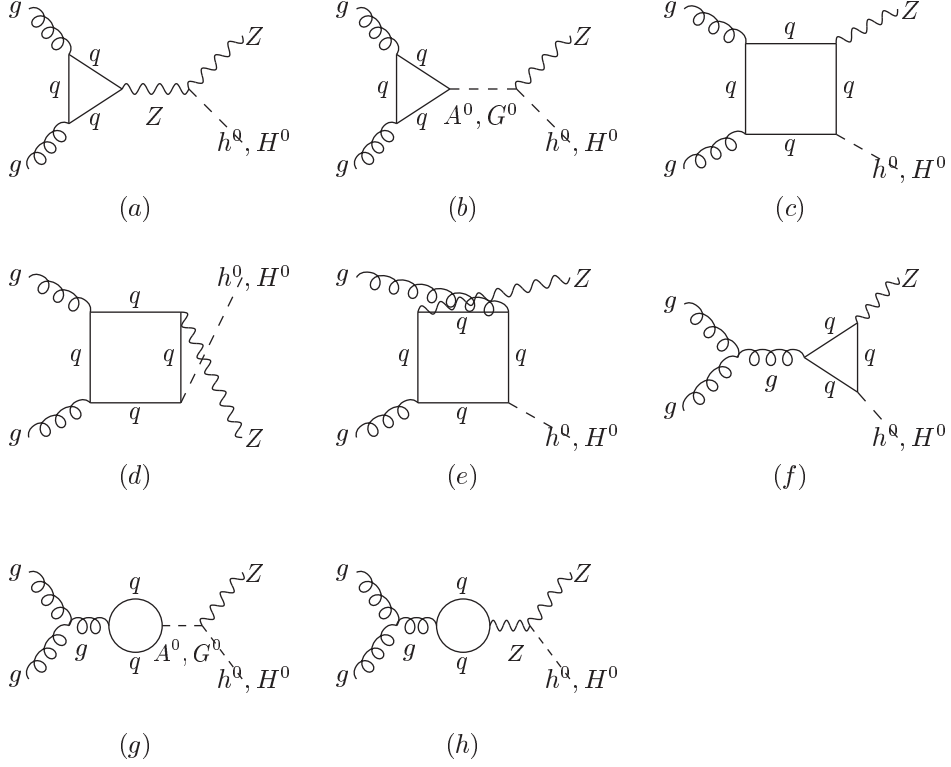


FIG. 2: Feynman diagrams for the subprocess $gg \rightarrow ZH$ (including only quark loop)

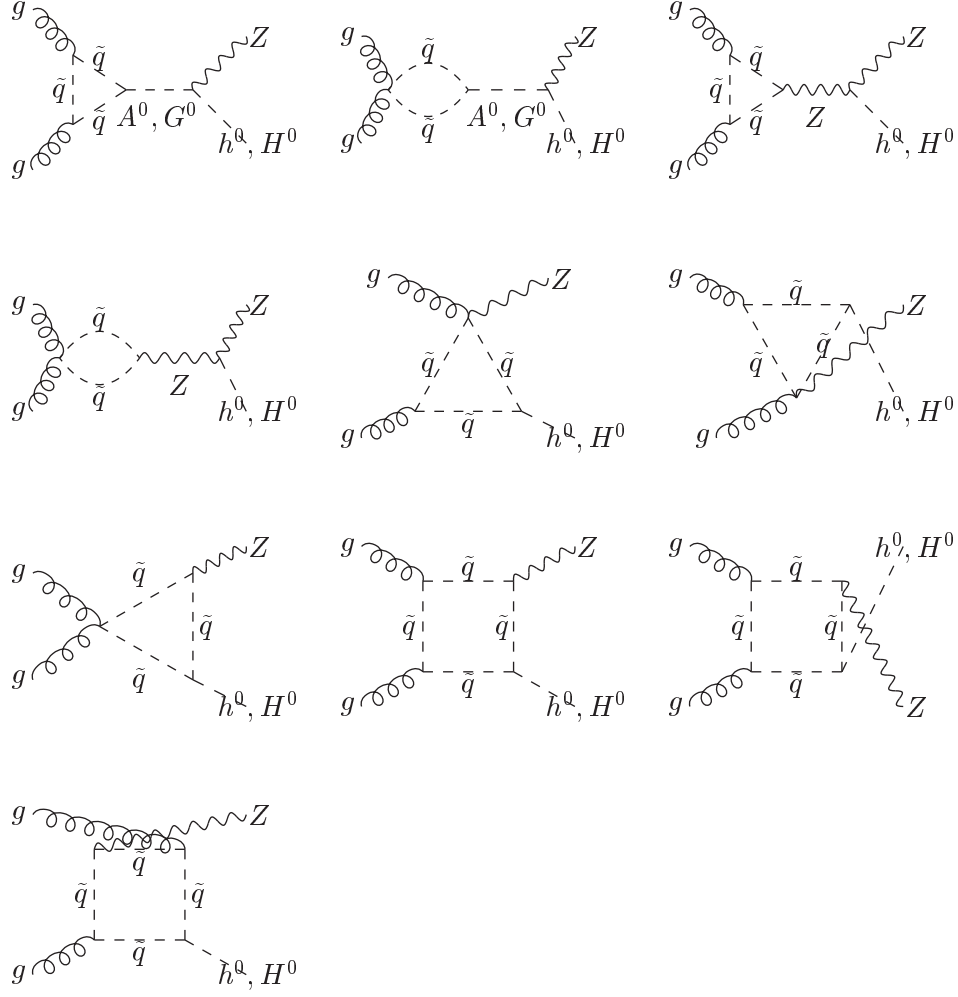


FIG. 3: Feynman diagrams for the subprocess $gg \rightarrow ZH$ (including only squark loop)

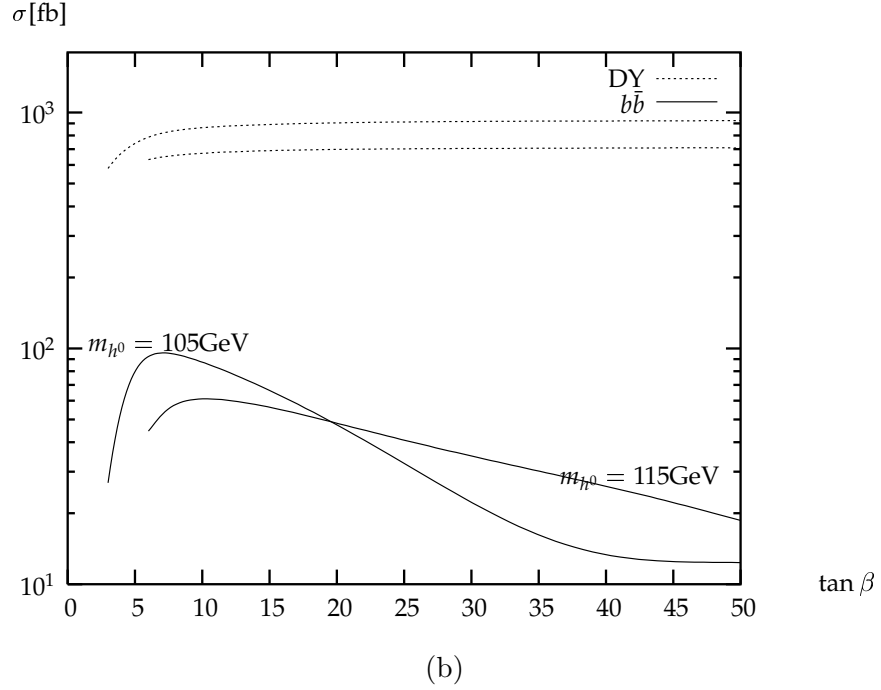
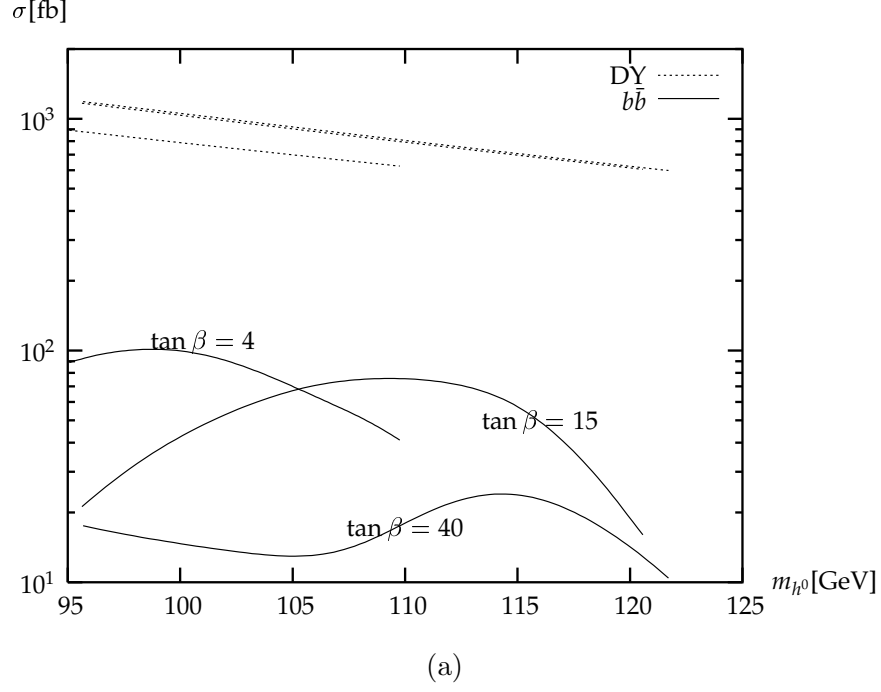


FIG. 4: Total cross sections σ (in fb) of $pp \rightarrow Zh^0$ via $b\bar{b}$ annihilation (solid lines) compared with Drell-Yan ones (dotted lines) at the LHC (a) as functions of m_{h^0} for $\tan \beta = 4, 15$ and 40 ; and (b) as functions of $\tan \beta$ for $m_{h^0} = 105$ and 115 GeV.

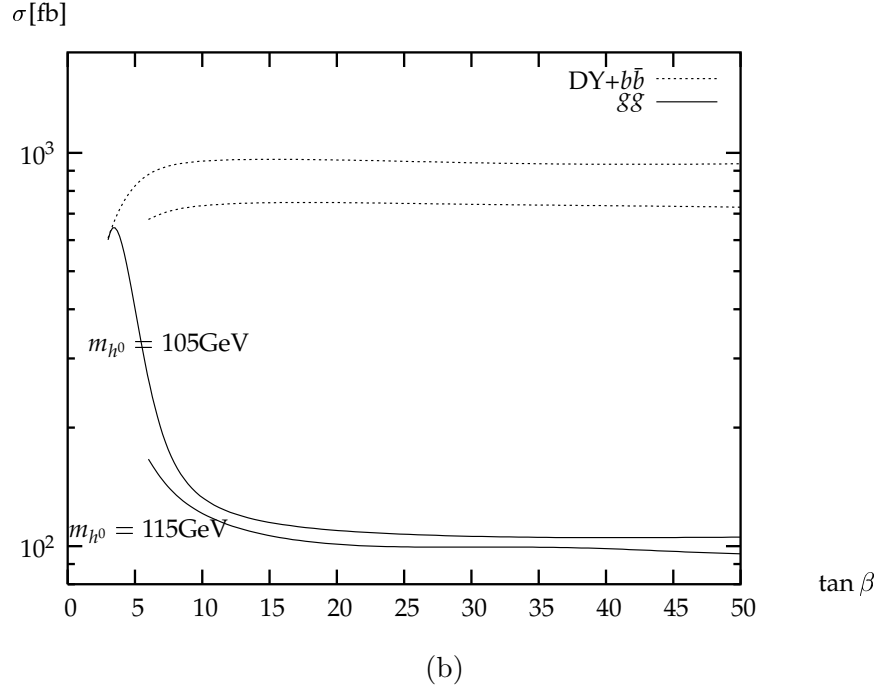
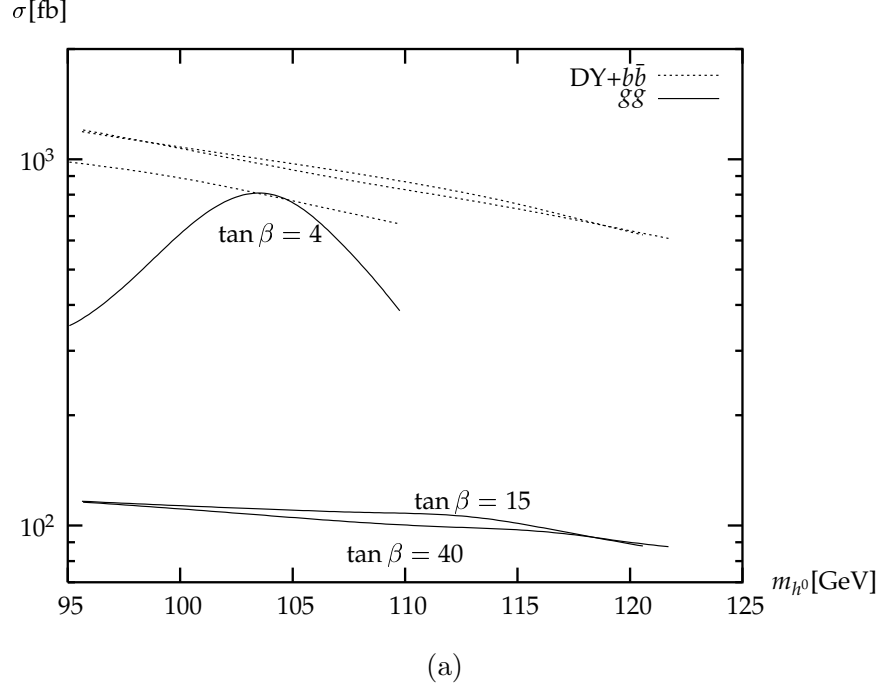
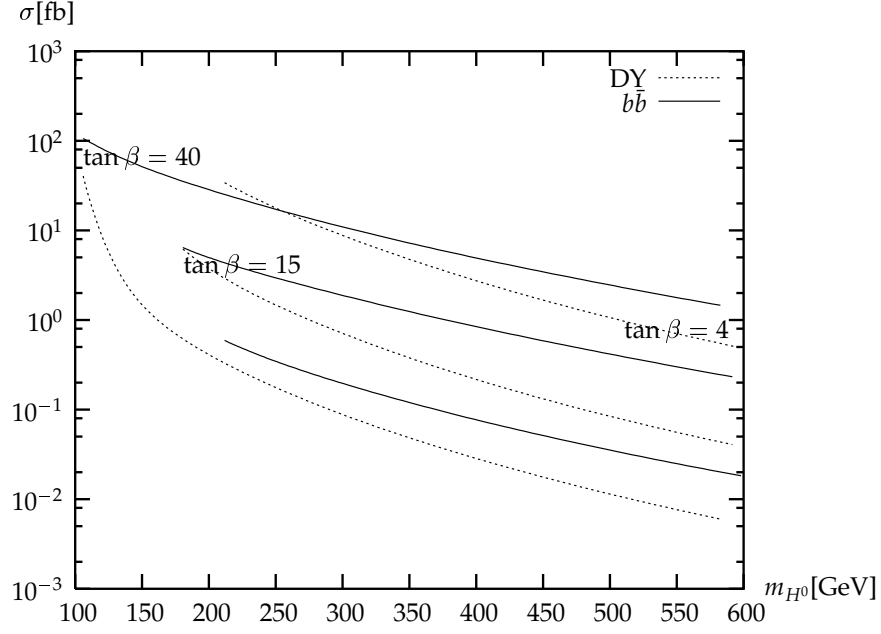
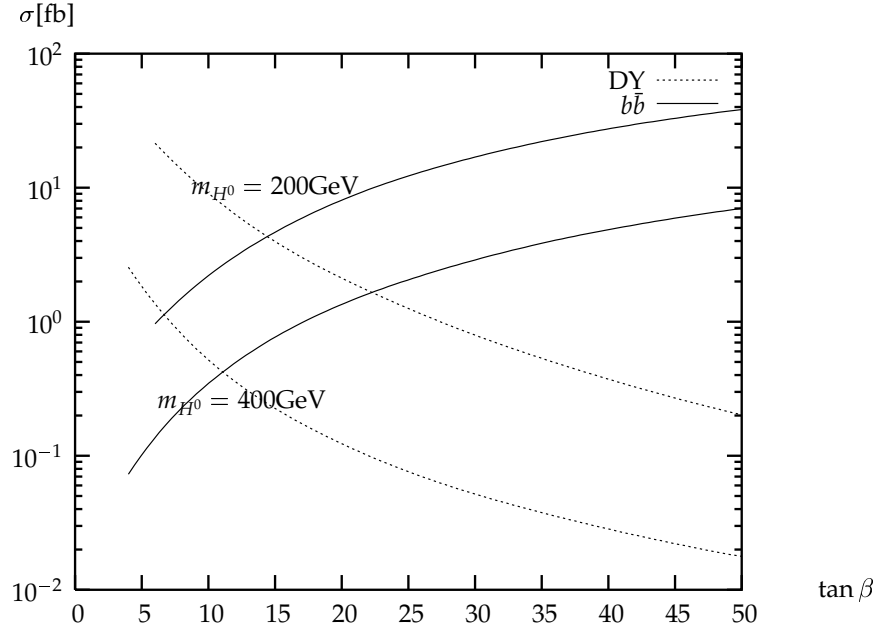


FIG. 5: Total cross section σ (in fb) of $pp \rightarrow Zh^0$ via gluon fusion (solid lines) compared with complete $q\bar{q}$ annihilation ones (dotted lines) at the LHC (a) as functions of m_{h^0} for $\tan\beta = 4, 15$ and 40; and (b) as functions of $\tan\beta$ for $m_{h^0} = 105$ and 115 GeV.

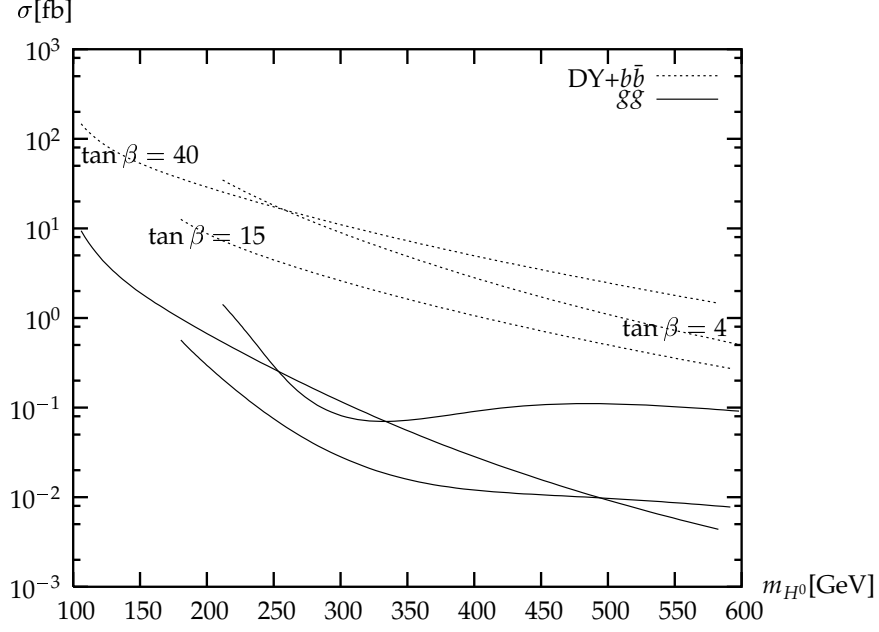


(a)

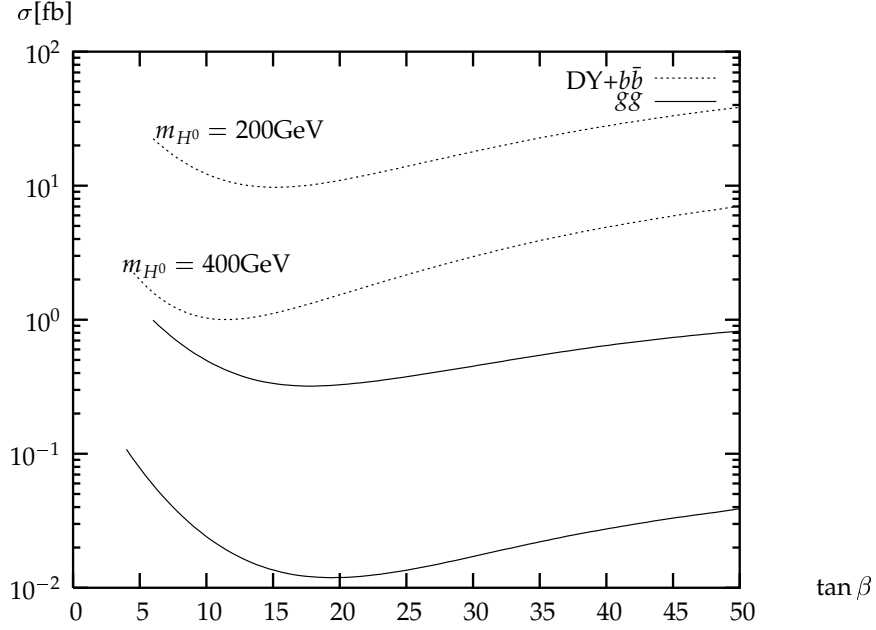


(b)

FIG. 6: Total cross sections σ (in fb) of $pp \rightarrow ZH^0$ via $b\bar{b}$ annihilation (solid lines) compared with Drell-Yan ones (dotted lines) at the LHC (a) as functions of m_{H^0} for $\tan\beta = 4, 15$ and 40 ; and (b) as functions of $\tan\beta$ for $m_{H^0} = 200$ and 400 GeV.



(a)



(b)

FIG. 7: Total cross section σ (in fb) of $pp \rightarrow ZH^0$ via gluon fusion (solid lines) compared with complete $q\bar{q}$ annihilation ones (dotted lines) at the LHC (a) as functions of m_{H^0} for $\tan\beta = 4, 15$ and 40 ; and (b) as functions of $\tan\beta$ for $m_{H^0} = 200$ and 400 GeV.

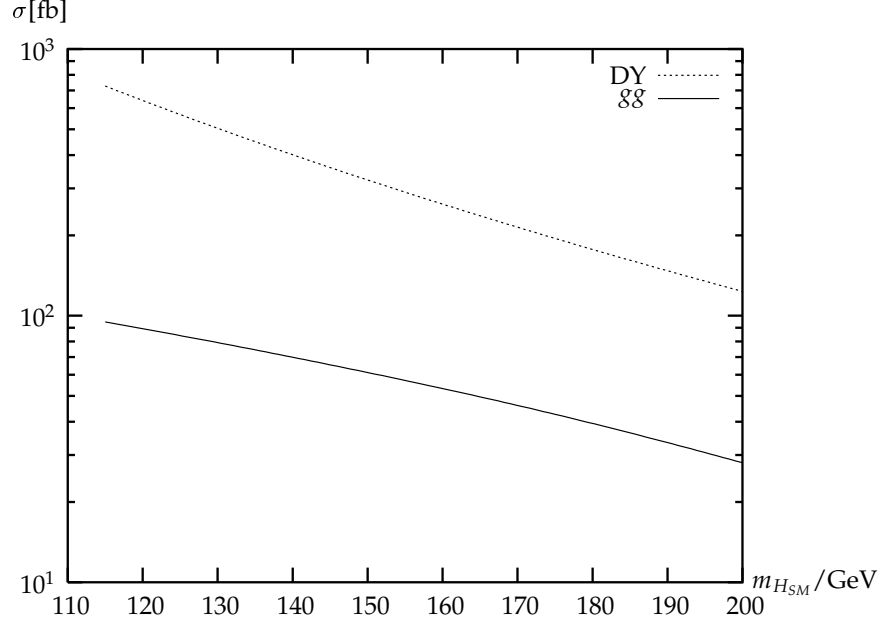


FIG. 8: Total cross sections σ (in fb) of $pp \rightarrow ZH_{SM}$ via gluon fusion (solid lines) compared with Drell-Yan ones (dotted lines) at the LHC as functions of standard model Higgs mass.

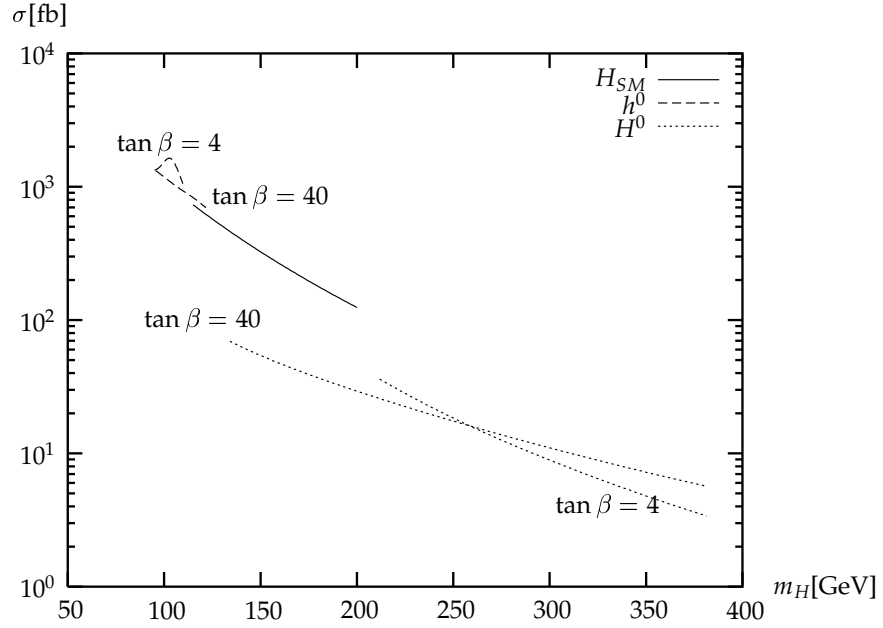


FIG. 9: A comparison of the production cross sections of the three Higgs bosons as functions of their masses.